



## Research Article

# Network-based analysis of heterogeneous patient-matched brain and extracranial melanoma metastasis pairs reveals three homogeneous subgroups

Konrad Grützmann<sup>a</sup>, Theresa Kraft<sup>a</sup>, Matthias Meinhardt<sup>b</sup>, Friedegund Meier<sup>c,d</sup>, Dana Westphal<sup>c,d</sup>, Michael Seifert<sup>a,d,\*</sup>

<sup>a</sup> Institute for Medical Informatics and Biometry, Faculty of Medicine, TU Dresden, 01307 Dresden, Germany

<sup>b</sup> Department of Pathology, University Hospital Carl Gustav Carus Dresden, TU Dresden, 01307 Dresden, Germany

<sup>c</sup> Department of Dermatology, University Hospital Carl Gustav Carus Dresden, TU Dresden, 01307 Dresden, Germany

<sup>d</sup> National Center for Tumor Diseases (NCT), D-01307 Dresden, Germany

## ARTICLE INFO

## Keywords:

Computational cancer biology  
Melanoma metastasis  
Gene regulatory network inference  
Network-based impact propagation  
Personalized network-based gene expression  
and promoter methylation data analysis

## ABSTRACT

Melanoma, the deadliest form of skin cancer, can metastasize to different organs. Molecular differences between brain and extracranial melanoma metastases are poorly understood. Here, promoter methylation and gene expression of 11 heterogeneous patient-matched pairs of brain and extracranial metastases were analyzed using melanoma-specific gene regulatory networks learned from public transcriptome and methylome data followed by network-based impact propagation of patient-specific alterations. This innovative data analysis strategy allowed to predict potential impacts of patient-specific driver candidate genes on other genes and pathways. The patient-matched metastasis pairs clustered into three robust subgroups with specific downstream targets with known roles in cancer, including melanoma (SG1: *RBM38*, *BCL11B*, SG2: *GATA3*, *FES*, SG3: *SLAMF6*, *PYCARD*). Patient subgroups and ranking of target gene candidates were confirmed in a validation cohort. Summarizing, computational network-based impact analyses of heterogeneous metastasis pairs predicted individual regulatory differences in melanoma brain metastases, cumulating into three consistent subgroups with specific downstream target genes.

## 1. Introduction

Melanoma, which develops from the pigment-producing melanocytes of the skin, is the most aggressive and deadliest form of skin cancer. While the five-year survival for localized melanoma is nearly 100 %, once metastasized, survival drops to 20 %. There are about 100,000 new melanoma cases and 6850 corresponding deaths per year in the US [1]. Exposure to sun light is a very strong risk factor especially for light-skinned people. UV radiation-induced mutations are the main cause of melanoma [2], but low percentages of cases are also of hereditary origin and show distinct mutational profiles [3]. Melanomas are known to have one of the highest mutation rate among all cancers resulting in strong patient-specific alterations [4]. MAPK signaling is the most commonly altered pathway in melanoma involving *BRAF* and *NRAS* as frequently mutated driver genes. Constitutive MAPK signaling activation leads to unrestricted proliferation. PI3K/Akt and mTOR

signaling are further frequently affected pathways. In addition, differentiation and cell death are disturbed in melanoma [5].

Primary melanoma are surgically removed accompanied by sentinel lymph node biopsy in high-risk melanoma. However, for metastatic melanoma, chemotherapy has been the only treatment option for decades without survival benefit. More recent targeted therapies like BRAF and MEK inhibitors have improved this considerably, e.g. the five-year overall survival rate for the BRAF/MEK inhibitor combination encorafenib plus binimetinib is 34.7 % [6]. However, the majority of patients develop resistance to such treatments [5]. Usually, the immune system recognizes and destroys tumor cells, but melanomas often develop evasion mechanisms. These include excretion of TGF- $\beta$  and suppressive cytokines, as well as PD-1 immune checkpoint protein over-expression [7]. With increasing knowledge about cancer-immune system interaction, new therapy options involving the immune system have been developed over the past 20 years [8]. While Interleukin-2 treatment

\* Corresponding author at: Institute for Medical Informatics and Biometry, Faculty of Medicine, TU Dresden, 01307 Dresden, Germany.

E-mail address: [michael.seifert@tu-dresden.de](mailto:michael.seifert@tu-dresden.de) (M. Seifert).

<https://doi.org/10.1016/j.csbj.2024.02.013>

Received 6 November 2023; Received in revised form 15 February 2024; Accepted 15 February 2024

Available online 17 February 2024

2001-0370/© 2024 The Authors. Published by Elsevier B.V. on behalf of Research Network of Computational and Structural Biotechnology. This is an open access article under the CC BY-NC-ND license (<http://creativecommons.org/licenses/by-nc-nd/4.0/>).

showed low response, new generation immunotherapy based on checkpoint inhibition can be considered a breakthrough for the treatment of metastatic melanoma [8]. Personalized molecular diagnostics and combination therapy have proven beneficial in approaching patient and tumor heterogeneity [7]. For example, the immune checkpoint inhibitor combination nivolumab plus ipilimumab achieves long-term survival for about 50 % of patients with metastatic melanoma (melanoma-specific survival rate of 55 % at 7.5 years) [9]. However, the rate of severe toxicity is as high as 59 % [10], and 50 % of patients do not experience long-term survival. The majority of patients with metastatic melanoma develop new brain metastases or suffer brain metastasis recurrence [11]. While melanoma brain metastases initially respond to current therapy regimens, they often relapse faster than other organ metastases, leading to a dramatic decrease in overall survival [12,13]. This may be in part explained by inefficient drug crossing of the blood-brain barrier and by factors in the brain micro-environment [14–16]. Further, altered metabolic processes in brain metastases may also contribute to therapy resistance [17,18].

An advanced understanding of molecular mechanisms is needed to develop better therapies for aggressive melanoma brain metastases. Studies have begun to elucidate the genetic differences of brain and extracranial metastases only recently [19–21]. Targeted sequencing identified recurrent driver gene mutations in brain metastases that were absent in extracranial metastases (e.g. in *ARID1A*, *ARID2*, *SMARCA4*, *BAP1* and *BRAF*) [20]. Another larger study that compared melanoma brain metastases to primary melanomas and extracranial metastases also included a small analysis of gene mutations for eight patient-matched brain and extracranial metastasis pairs [22]. This study reported a higher *BRAF* mutation rate in brain compared to extracranial metastases, which was also supported by the few patient-matched pairs. Further, gene expression profiling of patient-matched melanoma metastases identified immunosuppression and enrichment of oxidative phosphorylation in brain metastases that might directly contribute to therapy resistance [21]. Moreover, especially the PI3K/Akt signaling pathway was found to be hyperactivated in melanoma brain metastases [15,16,23,24]. In addition, single cell transcriptome studies of melanoma brain metastases are emerging. Eight functional cell programs were identified in brain metastases that define a proliferative and an inflammatory archetype coexisting in each metastasis [25]. Melanoma brain metastases are more chromosomally unstable, adopt a neuronal-like cell state and are enriched for spatially variably expressed metabolic pathways compared to their extracranial counterparts [26].

Promoter methylation of genes is known to be inversely correlated with their expression, and differential methylation is considered a mechanism for expression regulation [27]. Epigenetic alterations play a significant role in metastases formation of many cancers [28], including melanoma [29–31]. DNA methylation can not only greatly differ between patients but also between intra- and extracranial melanoma metastases of the same patient [31], leading to expression changes that may be involved in brain metastases formation [24,32]. Studying the interplay of the many omics layers allows for a better understanding of tumors as systemic disease, thereby advancing knowledge about their biology [33,34] and finding new treatment options [35]. Gene regulatory networks are appropriate tools to study complex processes like development and disease [36–38]. In the past, we successfully used gene network inference based on gene expression and copy number data in combination with network propagation strategies to predict cancer-relevant target genes [39–42]. Such network-based approaches could also help to jointly analyze the virtually private promoter methylation and gene expression profiles that distinguish patient-matched brain from extracranial melanoma metastases.

Here, we utilize gene expression together with promoter methylation data of 270 melanoma patients from The Cancer Genome Atlas (TCGA) to derive melanoma-specific gene regulatory networks. These networks were used to predict potential downstream impacts of genes with differentially methylated promoters and altered expression in a

heterogeneous patient-matched cohort of brain and extracranial melanoma metastasis pairs from seven patients (Fig. 1). This allowed to identify characteristic commonalities and differences between the metastasis pairs.

## 2. Materials and methods

### 2.1. Data and code availability

This paper analyzes existing, publicly available data from TCGA [43]. In addition, processed datasets derived from these data are available within the article, its [supplemental information](#), or have been deposited at Zenodo (doi: 10.5281/zenodo.10580565). All original code has been deposited at GitHub ([https://github.com/konradgrutz/MelBrainSys\\_networks](https://github.com/konradgrutz/MelBrainSys_networks), doi: 10.5281/zenodo.10582248) and is freely available.

### 2.2. Experimental model and subject details

The seven patients of the discovery cohort and the nine patients of the validation cohort with a brain and an extracranial melanoma metastasis were collected between 1994 and 2016 at the University Hospital Dresden (Dresden, Germany). Age and gender of subjects are provided in [Table 1](#) and S15. Most patients had not received any of the current state-of-the-art therapies, but were mostly untreated or treated with adjuvant IFN- $\alpha$  or chemotherapeutic drugs. Written informed consent was obtained for the use of tumor material for different molecular analyses and was approved by the ethics committee of the University of Dresden (Dresden, Germany) (EK 48022018). The studies were conducted in accordance with the Declaration of Helsinki.

### 2.3. Promoter methylation and gene expression data of patient-matched melanoma metastasis pairs

Processed DNA-methylation and gene expression data of 11 patient-matched brain and extracranial metastasis pairs from seven melanoma patients of the studies by Kraft et al. [32] and Westphal et al. [44] were considered (discovery cohort). Corresponding promoter methylation levels were determined for each included protein-coding gene by averaging the log<sub>2</sub>-ratios of the methylated to unmethylated signal of each of its promoter-associated CpGs. The average promoter methylation levels and the corresponding gene expression levels of the individual metastases are provided in [Table S1](#). We defined potential transcriptional driver genes for each patient-matched metastasis pair. These were genes that showed differentially decreased (increased) methylation of at least 20 % of its promoter-associated CpGs and at least a trend to an increased (decreased) expression in the brain compared to the corresponding extracranial metastasis. To realize this, differential CpG methylation was taken from the predictions of Kraft et al. [32] excluding promoters with opposite predictions for methylation states. The identified genes with differentially methylated promoters and resulting opposing expression are provided in [Table S2](#). These transcriptional driver candidates could act as potential source genes influencing the expression of other target genes. This will be analyzed with the help of gene regulatory networks described in the next sections.

### 2.4. Melanoma gene expression and promoter methylation data from TCGA for network inference

Microarray-based DNA-methylation and RNA-Seq gene expression data from the skin cutaneous melanoma (SKCM) cohort of The Cancer Genome Atlas (TCGA) were downloaded from [https://gdac.broadinstitute.org/runs/stddata\\_2013\\_11\\_14/data/SKCM/20131114/](https://gdac.broadinstitute.org/runs/stddata_2013_11_14/data/SKCM/20131114/). This cohort consists of primary and metastatic melanomas including one brain metastasis [43]. Only patient samples with a tumor content of at least 80 % were considered (TCGA variable “Tumour content (%)” %

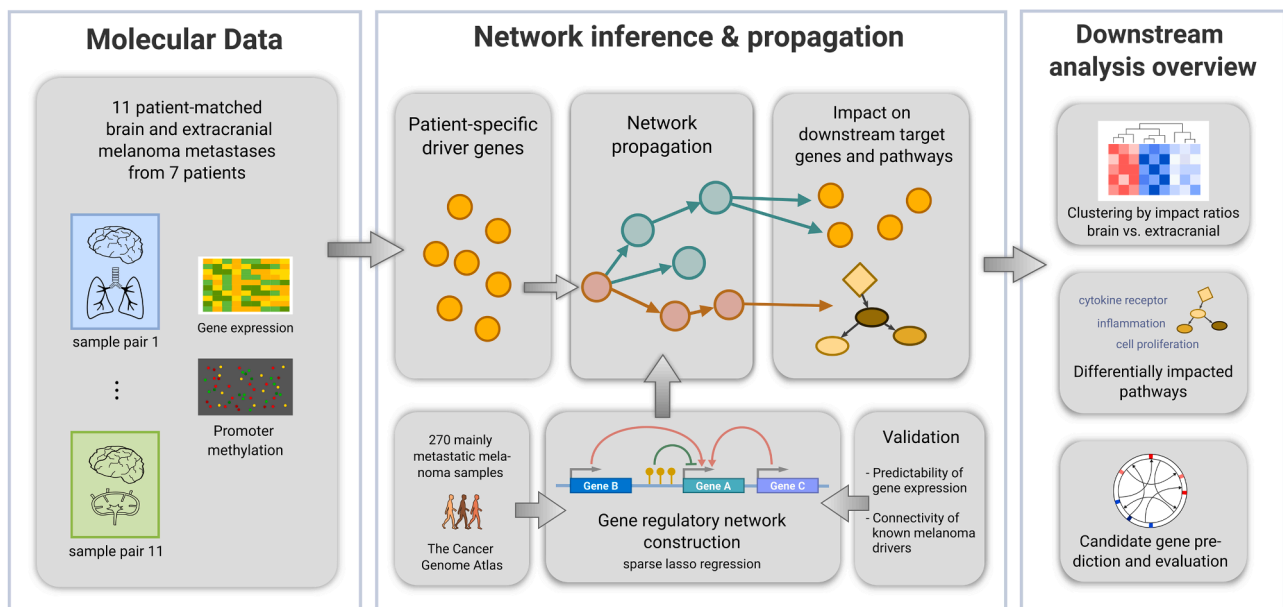


**Fig. 1.** Underlying data analyses workflow of this study. Left box: RNA-Seq gene expression and array-based promoter methylation were determined for 11 patient-matched brain and extracranial melanoma metastases of seven patients. Middle box: Patient-specific candidate driver genes with differential promoter methylation and opposed expression were determined for each metastasis pair. A melanoma-specific gene regulatory network was learned from data of The Cancer Genome Atlas (TCGA) and validated. Impacts of the driver genes on downstream target genes and pathways were elucidated via network propagation. Right box: Selection of performed downstream analyses. Average impact ratios were used for patient clustering resulting in three subgroups. Differentially impacted pathways were determined for each subgroup. Finally, target gene candidates were predicted for each subgroup and evaluated via literature research and an independent validation cohort.

**Table 1**

Clinical information of melanoma metastasis patients. For each patient one brain metastasis sample and one up to three extracranial metastasis samples were available. P followed by a number in the sample names represents patients, letters stand for tissues: brain (B), lung (Lun), skin (Ski), soft tissue (Sof), lymph node (Lym). The last columns indicate mutation statuses, where wt means wild-type. All statuses were from panel sequencing, except BRAFV600wt of patient P18, where only V600 was probed with PCR.

Patient	Extracranial samples	Sample pair IDs	Treated tissue	Gender	Age at brain surgery	Mutation status brain metastasis		Mutation status extracranial metastasis	
						<i>BRAF</i>	<i>NRAS</i>	<i>BRAF</i>	<i>NRAS</i>
P03	1 x lung	P03_BLun	none	female	55	BRAFV600E	wt	BRAFV600E	wt
P04	1 x skin	P04_BSKI_1	none	male	63	wt	wt	wt	wt
P08	3 x soft tissue	P08_BSof_1	both	male	73	wt	NRASQ61H	wt	NRASQ61H
		P08_BSof_2							
		P08_BSof_3							
P16	1 x lung	P16_BLun	none	male	84	wt	wt	wt	wt
P18	2 x lung	P18_BLun_1	none	male	69	BRAFG469R	wt	BRAFV600wt	wt
		P18_BLun_2							
P39	1 x lung	P39_BLun	both	female	63	wt	NRASQ61K	wt	NRASQ61K
P42	2 x lymph node	P42_BLYm_1	intracranial	male	70	wt	NRASQ61H	wt	NRASQ61H
		P42_BLYm_2							

nuclei that are tumour cells (0–100%)”, Table S3). The chosen tumor content cutoff ensures a good balance between high tumor content and enough samples to learn genome-wide melanoma-specific gene regulatory networks. The resulting raw gene expression counts of 270 patients were normalized by cyclic loess normalization (voom method of the R package limma, 3.42.2 [45]) and only genes with more than one count per million (CPM) reads in at least 50 % of the patients were kept. DNA-methylation data was cleaned up for CpGs covered by polymorphic or off-target probes based on data from McCartney et al. [46] and only CpGs in promoters of protein-coding genes that were also measured on our Illumina EPIC array were kept. Average methylation of a promoter was determined by computing the mean of its CpG measurements, which were given by CpG-specific log<sub>2</sub>-ratios of methylated to unmethylated signals. This resulted in a final data set that contained gene expression levels and corresponding average promoter methylation levels of 8251 genes for 270 melanoma patients (Table S3).

## 2.5. Melanoma-specific gene regulatory network inference

Melanoma-specific regulatory networks were learned from gene expression and promoter methylation data (Table S3) using the R package regNet [39]. A schematic flowchart of this process is shown in Fig. S1. For each target gene  $i$ , it is assumed that the expression level  $e_{id}$  of gene  $i$  in a melanoma sample  $d$  can be predicted by the linear combination  $e_{id} = a_{ii}m_{id} + \sum_{j \neq i} a_{ji}e_{jd}$  of its gene-specific promoter methylation  $m_{id}$  and the expression levels  $e_{jd}$  of all other potential regulator genes  $j \neq i$ . The unknown parameters  $a$  of the gene-specific linear model were learned from the TCGA data by regNet using lasso regression [47] in combination with a significance test for lasso [48]. The basic concept of this network inference approach has already been shown to perform well in similar network inference tasks [39–42]. In addition, lasso-based methods have been reported to be among the top performers for robust gene regulatory network inference [49]. The regNet parts that modeled

gene copy number alterations were used directly to model the promoter methylation. The sparse lasso regression enabled the selection of only those predictors (promoter methylation and/or expression levels) that best predicted the expression level of a specific target gene, while keeping the number of predictors small by setting the parameter values of irrelevant predictors to zero. This was done for each of the 8251 genes to obtain a global network. Only network edges between target genes and predictors that had a false discovery rate  $< 10^{-4}$  were kept. Further, the expression of genes in close vicinity is known to be correlated in global fashion, rather independent of specific regulation [50], which we confirmed in our data (Fig. S3). Therefore, potentially existing network edges from the 30 genes up- and downstream of a target gene were removed to avoid the inclusion of potentially spurious regulators as done in [39]. Note, regulatory connections in the model can also arise from mere correlation or indirect molecular interactions and do not necessarily reflect direct transcriptional regulation. Network inference was repeated 25 times by randomly selecting 75 % of the TCGA samples (202 patients) as training set on a compute server with Intel® Xeon® Gold 6230 CPUs. The inference of the 25 networks took a total of 155 h, applying an average of 75 CPUs with peaks of 260 GB RAM. Quantitative results were mainly reported as medians over the results obtained for the 25 individual networks. Further, each trained network was shuffled into 10 random network instances of same complexity by network permutations that keep the in- and out-degree of genes constant. These random network instances were considered for evaluation purposes with the remaining 25 % test data (68 patients) to obtain a base line for comparisons to the predictions of the original learned networks. To evaluate the trained networks, the expression values of the test data were predicted with the trained and the random network models and Pearson correlations with the originally measured values were calculated. Medians of Pearson correlations were calculated over all networks. It was further tested if the correlations were significantly greater than zero (*t*-test).

## 2.6. Computation of potential impacts of altered driver gene candidates on downstream target genes by network propagation

Considering the learned melanoma-specific network, the potential impact of an altered potential driver gene on a target gene's expression results from the direct and indirect network connections of both genes via other genes through network paths. The network propagation algorithm implemented in regNet [40] was used to compute patient-specific absolute impacts for each pair of genes for each of the 25 learned melanoma-specific networks considering the gene expression and promoter methylation profile of each melanoma metastasis of our cohort ( $pValCutoff = 0.01$ ,  $localGeneCutoff = 30$ ,  $colSumsThreshold = 10^{-3}$ ). This network propagation algorithm has already been successfully applied in similar studies to determine potential impacts of patient-specific gene mutations on patient survival [39], to identify potential driver gene candidates for oligodendrogliomas [42], and to predict genes associated with radioresistance [41]. The obtained impact matrices were used to realize different analyses as shown in the schematic flowchart in Fig. S2. For each melanoma metastasis, average impacts of each corresponding driver gene on the genes of each pathway of interest were computed. Then, the median values over the 25 networks were calculated. Afterwards, the log<sub>2</sub>-ratios of these medians in the brain versus the extracranial metastasis of each metastasis pair were calculated. Finally, the log<sub>2</sub>-ratios were averaged over all driver genes (upper right part of Fig. S2). A slightly different strategy was used for functional overrepresentation analyses, search of gene candidates and circos plots (lower part of Fig. S2). Pairwise impacts of each altered driver gene on each target gene were computed for each melanoma metastasis. Then the medians over all 25 networks were calculated. This yielded a matrix of median impacts of each driver gene on each target gene for each metastasis. Next, log<sub>2</sub>-ratios of these medians in the brain versus the extracranial metastases of each metastasis pair were

calculated and then used for further analyses. Conceptionally, it is sufficient to know that impact is the regulatory influence of a gene on another gene, or on a whole set of genes. The impact log<sub>2</sub>-ratio is the ratio of this influence between brain and extracranial metastasis and specifies if the impact is higher (log<sub>2</sub>-ratio  $> 0$ ) or lower (log<sub>2</sub>-ratio  $< 0$ ) in the brain compared to the corresponding extracranial metastasis.

## 2.7. Clustering of metastases according to pathway impact profiles

Impacts of metastasis pair-specific potential driver genes on entire cancer-relevant pathways of interest were determined to perform a hierarchical clustering of the individual metastasis pairs according to their obtained pathway impact profiles. Therefore, the previously determined impact log<sub>2</sub>-ratios computed by the network propagation algorithm for each metastasis pair (Methods Section 2.6) were considered for each metastasis pair to compute for each specific pathway its corresponding received impact by averaging the impact log<sub>2</sub>-ratios over all genes of this specific pathway (see schematic flowchart in Fig. S2). This was done for metabolic and signaling pathways based on initial gene lists from [39], which were updated by more recent information from ConsensusPathDB [51,52]. Additionally, immune pathways from the KEGG pathway database [53] were considered (Table S4). This resulted in metastasis pair-specific pathway impact profiles consisting of the average ratios of the impacts on the individual pathways. Hierarchical cluster analyses were done with these profiles to find metastasis pair subgroups using the R package pheatmap [54] with Euclidean distance and complete linkage. Further, corresponding cluster stability analyses were done with the R package pvclust [55] using standard parameters. The resultant AU-values for each subcluster are approximate p-values in percent, where a value of 100 indicates a completely stable subcluster. The three identified robust metastasis pair subgroups were used to guide the subsequent analyses.

## 2.8. Identification of overrepresented pathways and gene ontology terms for the three revealed impact subgroups

Gene-wise impact log<sub>2</sub>-ratios from the altered potential driver genes on all target genes were averaged over all altered genes of a metastasis pair (schematic flowchart in Fig. S2). Then the top (bottom) 5 % of target genes with highest (lowest) mean impact log<sub>2</sub>-ratios were taken, while only positive (negative) log<sub>2</sub>-ratios for top (bottom) genes were considered. Genes were then subjected to overrepresentation analyses of KEGG pathways and gene ontology terms (all three categories) applying clusterProfiler [56] (v3.14.0) with a FDR  $< 0.1$ . Then, group-specific, overrepresented pathways were defined as being shared between at least two metastasis pairs of a subgroup (from the clustering mentioned above), but not appearing in any other metastasis pair.

## 2.9. Identification of top gene candidates and creation of circos plots

Median impact log<sub>2</sub>-ratios were summarized over the patient-matched metastasis pairs of each of the three revealed pathway impact cluster subgroups to prioritize candidate target genes (schematic flowchart in Fig. S2). Only consistent target genes were considered with either positive or negative impact log<sub>2</sub>-ratios in all metastasis pairs of a subgroup. The mean median impact log<sub>2</sub>-ratio for each target gene over the metastasis pairs was calculated. Literature research (NCBI/pubmed, October 2022) was done for the top-ranking target genes focusing on those genes with the 10 highest and 10 lowest mean impact log<sub>2</sub>-ratios. Further, two text mining-based analyses were done with these gene lists: GEPI [57] was used for gene-gene interaction and single gene events with the keyword “melanoma” at sentence level, factuality “assertion”, and interaction types positive/negative regulation. Gene disease associations were retrieved from the DisGeNET platform using disgenet2r [58] and filtering the column “disease\_class\_name” for “neoplasm”. All interactions between potential driver and target genes of a subgroup's

metastasis pairs were further considered for visualization of the top-ranking target genes. The mean impact log<sub>2</sub>-ratio from potential driver genes was calculated in cases where a gene appeared in more than one metastasis pair. All resulting interactions were sorted by the number of metastasis pairs in which the potential driver gene appeared in and then by the absolute mean impact log<sub>2</sub>-ratio. Only the top 100 of these sorted interactions were kept. Three circos plots were created based on those interactions and genes using the R package circlize [59] (0.4.12), one for each of the three metastasis pair subgroups.

### 2.10. Validation of impact subgroups and subgroup specific target genes

We considered another cohort of patients, each with a brain and an extracranial melanoma metastasis, for validation (Table S15, validation cohort). Therefore, the same RNA sequencing and processing as for the discovery cohort was performed for nine additional patient-matched metastasis pairs, each with a brain and an extracranial melanoma metastasis. Expression log<sub>2</sub>-ratios between the brain and extracranial sample were determined for each metastasis pair, which was possible for 8184 (99.2 %) of the genes of the discovery cohort. The values of the remaining genes were set to zero (Table S15). A methylation matrix of genes and metastasis pairs was created that contained only zeros, corresponding to an absent methylation influence in the network regression models. Network propagation was done as described before, starting with all potential driver genes of all metastasis pairs of the discovery cohort to find corresponding downstream target genes and pathways in the validation cohort. Since only a small subset of 566 of all 8251 genes in the network had assigned promoter methylation as a predictor of their expression, the calculated impacts of genes were not significantly affected. Further, the fact that promoter methylation changes of a gene are also reflected in its expression level provides a backup for the network-based impact computations. Metastasis pair-specific profiles consisting of the average impact ratios between brain and extracranial metastases were used together with the profiles of the discovery cohort for cluster analyses done in the same manner as before. Further, all possible target genes were determined for the validation cohort as for the discovery cohort. As one of the subgroups had seven metastasis pairs, the constraint of a consistent impact ratio for target genes was relaxed: genes were considered consistent when six of the seven metastasis pairs showed a ratio into the same direction. The positions of the target gene candidates of the discovery cohort were determined in the ranked target gene lists of the validation cohort (Table S14).

## 3. Results

### 3.1. Strong molecular heterogeneity of melanoma metastases motivates a personalized network-based analysis of patient-matched metastasis pairs

Promoter methylation and gene expression profiles of patient-matched metastasis pairs of 11 melanoma brain and extracranial metastases from seven patients were used to search for potential driver genes that distinguish both metastases types (Table 1, Table S1, discovery cohort). The considered extracranial metastases occurred at different sites comprising lung, lymph node, skin and soft tissue. Multiple patient-matched pairs were available for three of seven patients (P08: 3 pairs, P18: 2 pairs, P42: 2 pairs), because histologically distinct regions were marked by an experienced pathologist for the extracranial metastases of these three patients. Between 11 and 279 potential driver candidate genes with differential promoter methylation and corresponding opposite gene expression were identified for each individual metastasis pair (Table S2) [32]. Only three potential driver genes were shared by five metastasis pairs (*ENPP2*, *LDLRAD2*, *RFTN1*) and eight genes by four pairs (*CMBL*, *ESPN*, *FERMT3*, *IL12RB2*, *KLHL6*, *NLRP1*, *PHGDH*, *TJP2*). More potential driver candidates were shared between the matched pairs of patients for which distinct histological regions were available from the extracranial metastases (P08: three pairs, 11 genes

shared, P18: two pairs, 10 genes shared, P42: two pairs, 25 genes shared). However, 73 % of all driver candidates occurred in only one metastasis pair (Fig. S4). These different observations highlight a strong heterogeneity of the patient-matched melanoma metastases, but this also clearly indicates that common potential driver genes and their downstream impacts on molecular processes cannot be determined by such a basic search strategy under these conditions. Thus, gene alterations of patient-matched melanoma metastasis pairs should better be analyzed in the context of genome-wide gene regulatory networks to enable the prediction of commonly altered pathways in the cohort or in patient subgroups to better understand relevant molecular processes altered by the specific driver candidates of each metastasis pair.

### 3.2. Melanoma-specific gene regulatory networks learned from public data predict expression behavior of patient-matched metastases

Transcriptome and promoter methylation data of 270 melanoma patients (215 metastases including one brain metastasis, 55 primary tumors) of the TCGA skin cutaneous melanoma cohort were used to computationally infer a gene regulatory network for metastatic melanomas [43] (Table S3). For each of these patients, gene expression and corresponding promoter methylation levels of 8251 genes, which were also measured in our melanoma cohort, were utilized (Table S3). The network inference was done with the R package regNet [39], modeling the expression of each gene as a linear combination of the gene's own promoter methylation level and the expression levels of all other potential regulator genes (see schematic flowchart in Fig. S1). regNet utilizes sparse regression to predict for each gene the most relevant genes that best explain the expression of this gene across the patients. The resulting edges between genes form a gene regulatory network (Table S5). The network inference was repeated 25 times utilizing a training set of 202 of 270 (75 %) randomly chosen patients. The resulting networks had on average  $27,275 \pm 634$  directed edges between genes and on average the methylation levels of  $566 \pm 23$  promoters were selected to directly influence the expression of the associated genes (false discovery rate  $< 10^{-4}$  for included edges). About three quarters of the edges between genes were potential activator links and about one quarter were inhibitor links. Most of the links were between genes in relative close vicinity on the same chromosome, but there were also many links between genes of different chromosomes (Fig. S5). Furthermore, many known key drivers of melanoma development (*ATF3*, *BRAF*, *TET1*, *ARID2*, *DNMT3B*, *CTCF*, *FOS*, *DNMT3A*) [5, 60,61] were among the genes with the most outgoing edges to other genes and were therefore well embedded in the networks (Table S6).

Next, the learned networks were tested for their capability to predict the expression levels of individual genes. These predictions were performed separately for each network with its remaining 25 % of patients (68 of 270) that were not used during inference. Then the correlation between the predicted and the originally measured expression levels of each gene across all test patients was calculated. The vast majority of genes showed positive correlations suggesting that the underlying networks contain relevant information for the prediction of expression levels of genes in metastatic melanomas (Fig. 2A, median correlation  $r = 0.61$ ,  $p = 1.87 \cdot 10^{-8}$ , *t*-test). This was further supported by the fact that random networks of same complexity were not able to predict the expression levels of genes (Fig. 2A,  $r = 0.003$ ,  $p = 0.49$ , *t*-test).

Moreover, the learned networks were tested for their capability to predict the expression levels of individual genes in our melanoma metastases cohort. While the correlations between the network-based predicted and the originally measured expression levels were lower compared to those obtained for the TCGA test data, the majority of genes still showed positive correlations (Fig. 2A, discovery cohort median correlation  $r = 0.39$ ,  $p = 0.021$ , *t*-test). Stratification into brain and extracranial metastases revealed the same predictive power (Fig. 2B). Thus, despite only one brain metastasis in the TCGA cohort, the trained networks demonstrated effective generalization across metastatic

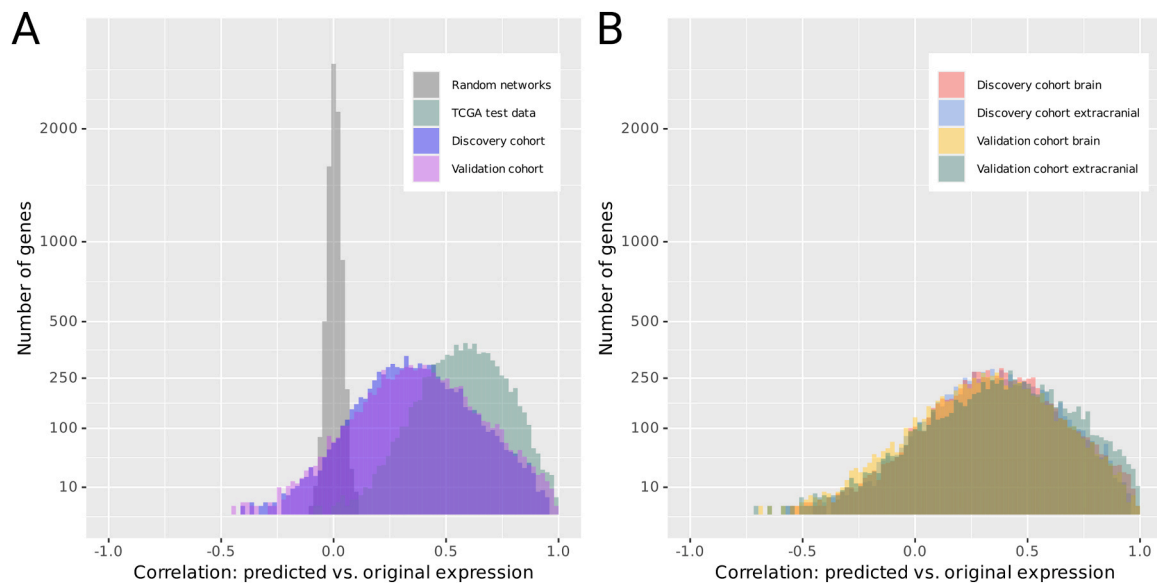


**Fig. 2.** Predictive performance of the learned melanoma-specific gene regulatory network. A: The correlations between predicted and originally measured gene expression levels quantify the predictive performance of the learned network for the TCGA test data by the inferred regulatory network (green), for the TCGA test data by the random networks (gray), and for the gene expression profiles of the patient-matched melanoma metastases in our discovery cohort (blue) and validation cohort (magenta) with the inferred network. The results shown are the medians over all 25 learned networks inferred from the TCGA training sets. The median correlations for the prediction of the TCGA test data ( $r = 0.61$ ,  $p = 1.27 \cdot 10^{-8}$ ,  $t$ -test), the discovery cohort ( $r = 0.39$ ,  $p = 0.020$ ) and the validation cohort ( $r = 0.42$ ,  $p = 0.041$ ) were significant, whereas random networks of the same complexity as the inferred networks were not able to predict the gene expression levels ( $r = 0.003$ ,  $p = 0.490$ ). B: Stratification into brain and extracranial metastases showed essentially the same predictive performance for the discovery (red and blue) and validation cohort (yellow and green). This proved that the learned gene regulatory networks generalized well over different metastatic tissues.

tissues. Thus, this clearly shows that for most genes the inferred melanoma-specific networks provide solid predictions, and the networks can therefore be utilized to analyze the patient-matched melanoma metastases of our cohort.

### 3.3. Impacts of pair-specific driver candidates on cellular pathways separate metastasis pairs into three subgroups

Next, the putative impacts of all potential driver candidate genes with differential promoter methylation and corresponding opposing gene expression of each patient-matched metastasis pair were determined (see schematic flowchart in Fig. S2). Therefore, the network propagation algorithm implemented in regNet [39] was applied. This algorithm predicts the influence of each driver gene on the expression of every other gene by considering all directed network paths between the genes, and the predictions for each gene along the path.

Since alterations of different cellular pathways are known to play important roles in melanoma metastases, the results of the network propagation were considered to determine the potential impacts of each altered driver gene on genes of signal transduction, metabolic and immune pathways (Table S4). This was done for each patient-matched brain and extracranial metastasis pair. Intuitively, the impact is the potential regulatory influence of a gene on a pathway. The impact log<sub>2</sub>-ratio is the ratio of this influence between the brain metastasis and the extracranial metastasis of a patient. The distribution of the impact log<sub>2</sub>-ratios differed from metastasis pair to metastasis pair. However, all these ratios mainly range from -5 to 5 indicating that the pair-specific driver candidates may influence the expression of specific pathway genes (Fig. S6).

Average impacts of all pair-specific driver candidates on each signaling, metabolic and immune pathway were computed to better characterize this at the level of individual pathways (Table S7, Fig. S2). A hierarchical clustering of these resulting pathway impact ratios revealed two phenomena that were consistent across all three pathway categories (Fig. 3). First, the pathways received impact ratios from the driver candidates that varied in their strength and directionality across

the 11 patient-matched metastasis pairs. Secondly, the patient-matched metastasis pairs were split into three homogeneous subgroups with highly consistent subgroup-specific impact ratios across all pathways. These subgroups showed on average rather higher (red, subgroup SG1), lower (blue, subgroup SG2) and slightly lower (light blue, subgroup SG3) impacts of driver candidates on pathways comparing brain to extracranial metastases (Fig. 3). A bootstrapping-based stability analysis was applied to assess the reliability, and thus, universality of the subgroups. It confirmed that these clusters were highly stable for signaling and immune pathways (Fig. 3: AU values of 100 for root nodes of subgroups) and for some subgroups less stable in the context of metabolic pathways (AU-values between 64 and 98 for root nodes of subgroups).

In addition, the assignment of patient-matched pairs to subgroups was very consistent between the three pathway categories, except for the metabolic pathways of metastasis pair P08\_BSof\_3 (Fig. 3). Generally, the metastasis pairs did not cluster according to the tissue type of the extracranial metastases. Moreover, several metastases of the patients with multiple pairs were even assigned to different subclusters (patients P08, P18 and P42). Thus, histologically distinct regions of a metastasis differed in their pathway impact profiles, which may result from different subclones within a metastasis.

### 3.4. Overrepresented functional terms of target genes influenced by potential driver candidates suggest regulatory differences between the three subgroups

The considered signaling, metabolic and immune pathways were affected in a similar manner within each of the three revealed metastasis pair subgroups (Fig. 3). An overrepresentation analysis was performed on the basis of gene ontology (GO) terms using clusterProfiler [56] to obtain a detailed overview which of the pathways were significantly enriched for differential impacts from the metastasis pair-specific driver candidates. To realize this, all potential target genes that received impacts from driver gene candidates via network propagation were ranked by their impact log<sub>2</sub>-ratios of the brain metastasis in relation to the corresponding patient-matched extracranial metastasis (see schematic

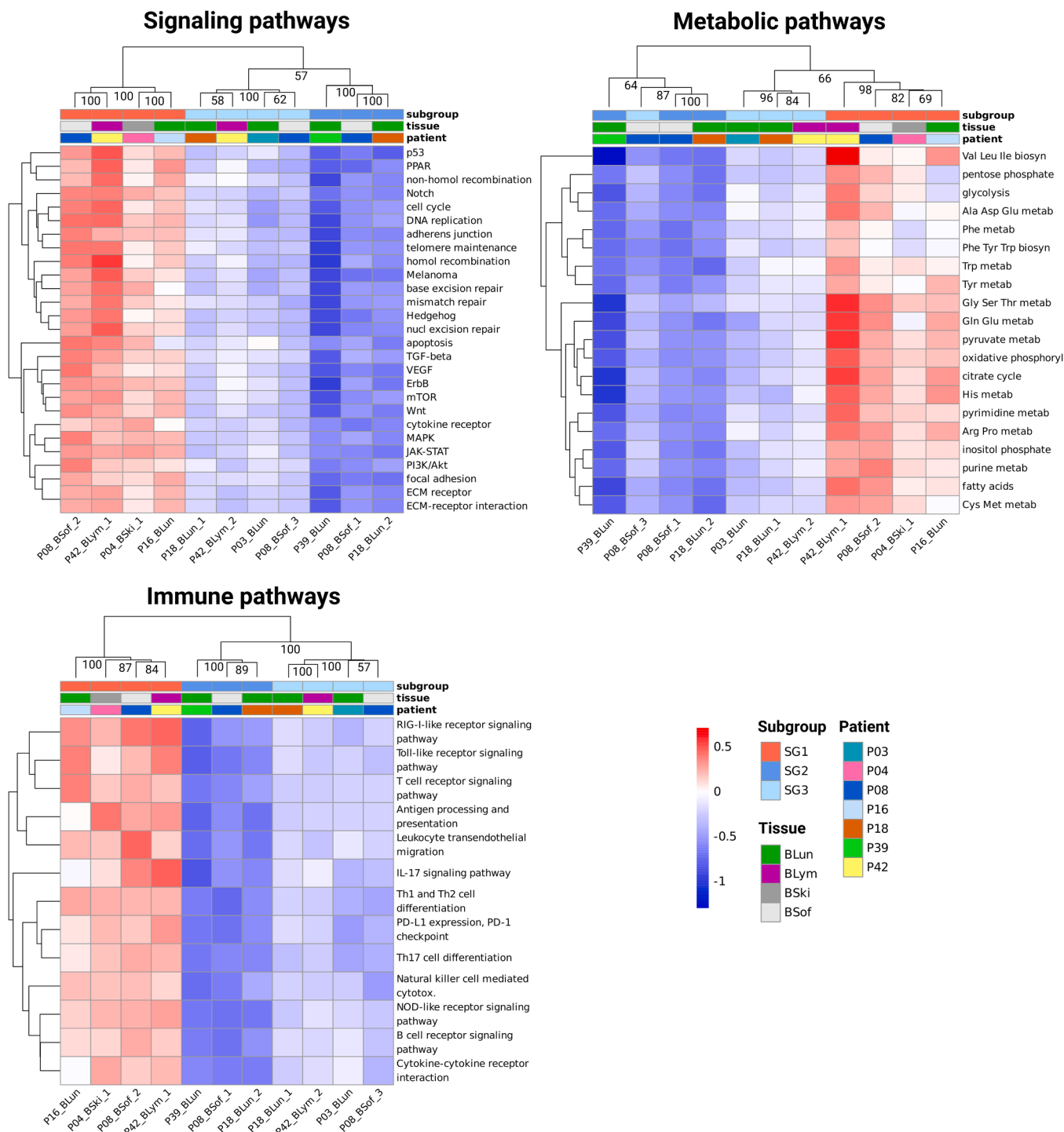


**Fig. 3.** Heatmap-based cluster analysis of pathway impact profiles of patient-matched metastasis pairs of the discovery cohort. The pathways were grouped into three separately displayed categories (signaling, metabolic, immune). For each pathway (row) the plotted values represent the average impact log<sub>2</sub>-ratios from all potential driver genes on all pathway genes for a specific metastasis pair (column). Red tiles in the heatmap represent higher and blue ones represent lower impacts in the brain compared to its corresponding extracranial metastasis. The metastasis pair names are shown below the heatmap where a P followed by a number represents the individual patient and the subsequent letters represent the two metastases of the pair: brain (B), lung (Lun), skin (Ski), soft tissue (Sof), and lymph node (Lym) (Table 1). The full pathway names are in Table S4 and the underlying data are contained in Table S7. The numbers shown in the dendrograms above the heatmap represent the approximately unbiased p-values (AU-values) from the corresponding cluster stability analysis, where a value of 100 means that the corresponding subcluster was completely stable.

flowchart in Fig. S2). Based on this ranking, the top 5 % of genes that received the highest impact log<sub>2</sub>-ratio (strong positive impact log<sub>2</sub>-ratio) and the top 5 % of genes that received the lowest impact log<sub>2</sub>-ratio (strong negative impact log<sub>2</sub>-ratio) were used for the over-representation analysis. This determined those molecular processes that

best distinguish each brain from its corresponding extracranial metastasis at a false discovery cutoff of 0.1 (Table S8). Next, subgroup-specific enrichments were selected based on the criterion that a specific enriched ontology term was found in at least two metastasis pairs of the subgroup, but not found to be enriched in any other metastasis pair of the two other

subgroups (Table 2, Table S8).

Overall, the subgroups SG2 and SG3 showed only few subgroup-specific overrepresented GO terms, which were observed for target genes that received lower impacts in brain compared to extracranial metastases. This included proteolysis and negative regulation of cell proliferation for SG2 and cytokine receptor activity for SG3. In contrast, SG1 was characterized by many subgroup-specific, overrepresented GO terms, including plasma membrane, cytokine signaling and interferon signaling which were all overrepresented among the target genes that received greater impacts in brain compared to extracranial metastases from the pair-specific driver genes. In addition, target genes that received lower impacts were enriched for GO terms associated with functions of the immune system (migration of immune cells, mast cell activity, inflammatory response), calcium ion transport, glial cell activation and PI3K signaling. Thus, subgroup-specific alterations of pathway activities triggered by potential driver candidate genes are likely to exist.

### 3.5. Associations between pathway expression and received impacts from driver candidates reveal subgroup-specific commonalities and differences

Next, we estimated how the impacts of the driver candidates influence the expression of individual pathways. Therefore, the impact on each pathway and the expression of each pathway were considered for each metastasis pair by comparing the brain to the corresponding extracranial metastasis. The correlation between impact and expression changes was calculated over all pathways for each metastasis pair (Fig. S7, Table S7). Except for two metastasis pairs (P08\_BSof\_1, P16\_BLun), all pairs showed moderate to strong negative correlations between the received average differential impacts and the average expression alterations of pathways in the brain compared to the corresponding extracranial metastases (Fig. 4). Especially the four observed

**Table 2**

Overrepresented GO terms exclusively shared within metastasis pair subgroups. Target genes with impact ratios in the upper 5 % (higher impact in brain) or lower 5 % (lower impact in brain) of each metastasis pair were analyzed by clusterProfiler [56] to obtain overrepresented GO terms (FDR < 0.1). Shown are the numbers of overrepresented GO terms that were shared between at least two metastasis pairs of each respective subgroup, where these terms did not appear in metastasis pairs of any other subgroup. The full result list is in Table S8.

Subgroup	Gene list	Number of overrepresented GO terms	Summary of overrepresented GO terms
higher in brain, SG1	upper 5 %	7	plasma membrane, cytokine signaling and interferon I signaling, defense response to virus
	lower 5 %	108	migration of diverse immune cells, mast cell activity, myeloid cell differentiation, PI3K signaling, superoxide metabolism, (neuro) inflammatory response, calcium ion transport and glial cell activation
slightly lower in brain, SG3	upper 5 %	0	
	lower 5 %	2	cytokine receptor activity
lower in brain, SG2	upper 5 %	0	
	lower 5 %	9	negative regulation of cell proliferation, (positive) regulation of proteolysis, cardiac chamber development / morphogenesis, development cardiac ventricle, aortic valve, ventricular septum and semilunar valve

strong negative correlations had all false discovery rates less than 0.031 (Fig. 4: P04\_BSk1\_1, P08\_BSof\_3, P39\_BLun and P42\_BLym\_1). Thus, increased impacts in the brain metastasis compared to the corresponding extracranial metastasis tend to be associated with a reduced expression of pathways, whereas decreased impacts in the brain metastasis may lead to an increased expression of pathways. This global inverse trend was consistent for all three subgroups SG1, SG2, and SG3 of the melanoma metastasis pairs (Fig. 4, Fig. S7).

Next, we were interested in pathways and their behavioral patterns, and whether a pattern recurred more frequently in certain subgroups. The behavior of a pathway is defined by its higher or lower expression and whether its received impact is higher or lower in the brain compared to the corresponding extracranial metastasis. A lower impact ratio means that the pathway was less influenced by the individual driver gene candidates in the brain compared to the extracranial metastasis of a patient. This behavior was predominantly seen in the metastasis pairs of the subgroups SG2 and SG3. Among these pathways were those with higher expression in the brain metastases, especially the pyruvate metabolism, the citrate cycle, and the pentose phosphate pathway. These pathways were more active in brain metastases, but their activity was less influenced by the potential driver genes. The other category of pathways less influenced by the driver genes were the less active ones (lower expression in brain). They included two pathways known to play a role in cytokine receptor signaling and other signaling pathways (e.g. MAPK, ErbB, and Wnt signaling) (Table S9).

On the other hand, pathways that received higher impact ratios were more influenced by the individual potential driver genes in the brain compared to the extracranial metastasis. This was primarily seen in subgroup SG1. Among these pathways were those with less activity (lower expression in brain), mainly including cancer signaling (e.g. PI3K/Akt, MAPK, and p53 signaling) and immune pathways (e.g. cytokine receptor, T cell receptor, and IL-17 signaling). These pathways were potentially downregulated by the candidate driver genes. Furthermore, there were pathways receiving higher impacts that were associated with increased expression in brain compared to corresponding extracranial metastases. These were mainly metabolic pathways (citrate cycle, pyruvate metabolism, amino acid metabolic pathways), mTOR signaling, non-homologous recombination and telomere maintenance (Table S9).

### 3.6. Differentially regulated candidate target genes are distinct between subgroups but potentially highly relevant for metastasis formation

Since metastasis pairs showed group-specific overrepresented pathways, it was further analyzed if single subgroup-specific target genes with consistent differential impacts between the brain and extracranial metastases exist. Therefore, subgroup-specific average impact log<sub>2</sub>-ratios were considered to determine the top 10 target genes with the highest and top 10 lowest impact ratios for each of the three subgroups SG1, SG2, and SG3 (Table S10, see schematic flowchart in Fig. S2). Opposed to the patient-matched metastasis pairs of the subgroup SG1, pairs of the two other subgroups, SG2 and SG3, only showed target gene candidates with consistently lower impact in brain metastases. Still, the three subgroups were nearly perfectly separated by the impact log<sub>2</sub>-ratios of the target candidates (Fig. S8) suggesting that the subgroup-specific top target genes are good general representatives of the subgroups. Overall, the received impact log<sub>2</sub>-ratios and corresponding expression log<sub>2</sub>-ratios of these top target candidates were positively correlated ( $r = 0.26$ ) indicating that expression alterations of the potential driver candidates triggered by promoter methylation alterations influence the expression of these top target genes.

Next, the 100 strongest and most consistent impacts on the subgroup-specific top target gene candidates and the corresponding potential driver genes were visualized for each of the three subgroups (Fig. 5, see Methods for selection criteria of displayed potential driver genes). This again confirmed the need and advantages of the performed network-based analysis, because the included potential driver genes were only

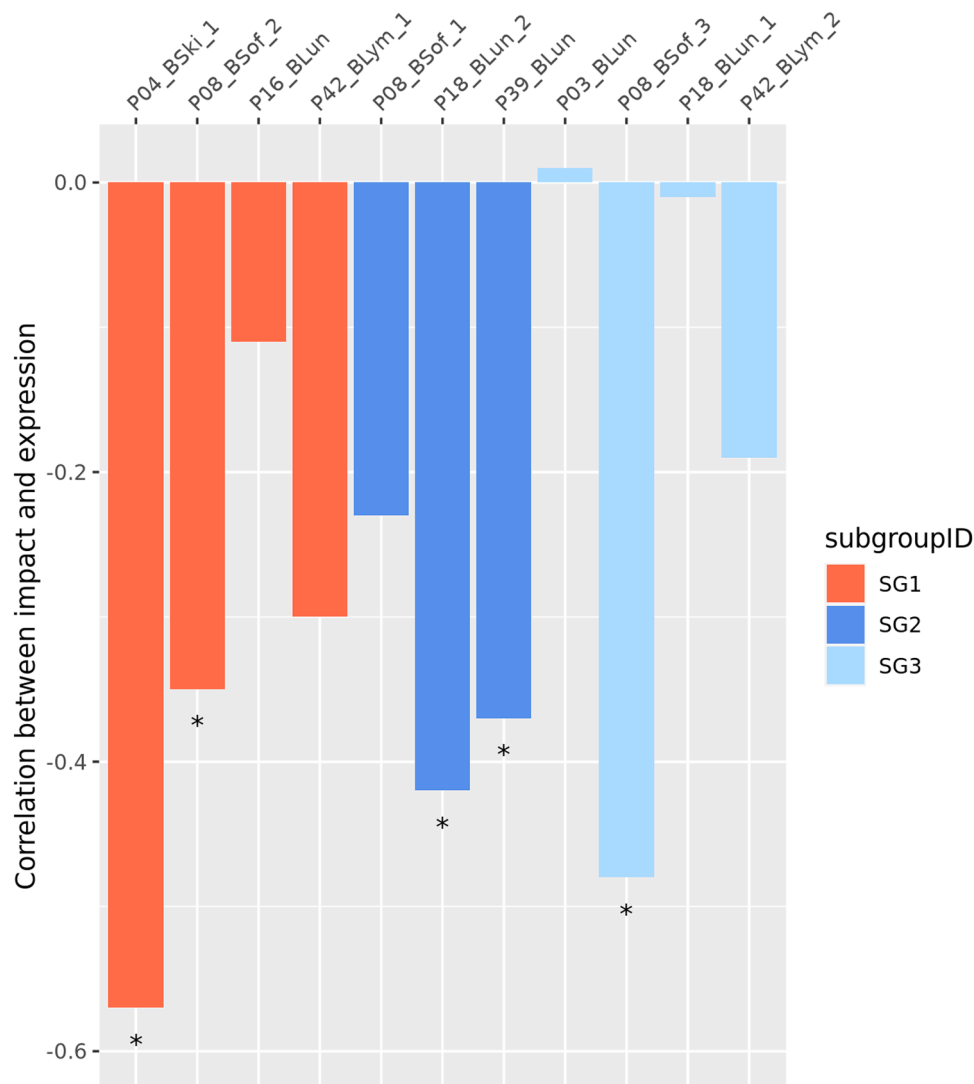


**Fig. 4.** Relation between impacts of potential driver genes on cellular pathways and pathway expression for the patient-matched metastasis pairs of the discovery cohort. For each cellular pathway (Table S4), the average impact log<sub>2</sub>-ratio of the potential driver genes on the pathway genes was computed using network propagation, and the average expression log<sub>2</sub>-ratio was calculated over all pathway genes. For both log<sub>2</sub>-ratios, the brain and the corresponding extracranial metastasis of each metastasis pair were compared. The displayed bars show the correlation between the impact and the corresponding expression log<sub>2</sub>-ratios over all considered pathways for each metastasis pair. For the majority of pairs, negative correlations were observed between the impacts on the pathways and the expression of the pathways, meaning that higher (lower) impacts in the brain metastasis were associated with reduced (increased) pathway expression compared to the corresponding extracranial metastasis. A star “\*” below a bar indicates the significance of the correlation (FDR-adjusted  $p < 0.05$ ,  $t$ -test). The corresponding scatter plots of the individual metastasis pairs are shown in Fig. S5 and the underlying data are contained in Table S9. The metastasis pair names are shown above the bars where a P followed by a number represents the individual patient and the subsequent letters represent the tissues of the two metastases of the pair: brain (B), lung (Lun), skin (Ski), soft tissue (Sof), and lymph node (Lym) (Table 1).

altered in one or two metastasis pairs, whereas their potential target genes were consistently differentially impacted within each subgroup. Thus, the subgroup-specific circo plots in Fig. 5 summarize the complex relationship between driver candidates and target genes connected through all possible network paths. They further enable to focus on the most relevant subgroup-specific target genes, which received the strongest impacts from the respective driver candidates. Overall, the three subgroups showed largely distinct sets of driver candidates and target genes. Only four target gene candidates (*BCL11B*, *GGCT*, *TLL7*, *SPAG16*) and no driver candidates were shared among the subgroups. Two text mining-based analyses indicated that nine target gene candidates had gene-gene interactions or single gene events in the melanoma context (Suppl. Table S11) and nine partially shared genes showed gene-disease associations with melanoma (Suppl. Table S12). Many more genes showed disease associations in the broader neoplasm context (Suppl. Table S12). Additionally, an extensive, manual literature review

showed that nearly all target gene candidates are associated with cancer, although with different degrees of evidence (Appendix A, Table S13). In total, 21 of the 40 genes showed associations with melanoma.

Table 3 shows a selection of the most promising target candidates for each subgroup (see full list in Table S13 and Appendix A). Many of them have known associations with melanoma metastasis formation. There were two genes for subgroup SG1 (Fig. 5A). *RBM38* is involved in DNA damage response [62] and promotes proliferation and invasion in melanoma [63]. *BCL11B* (also in SG2) is the master transcription factor for T cell identity, and there is support for its role in melanoma [64,65]. There were three very promising candidate genes for SG2 (Fig. 5B). *AIM2* regulates anti-tumor immunity and is a viable therapeutic target for melanoma [66]. *FES* is a driver of melanoma progression [67], and there is evidence that it is involved in metastasis formation in melanoma [68]. *GATA3* promotes invasive behavior in melanoma cells [69]. Finally, subgroup SG3 had two very promising target candidates (Fig. 5C).

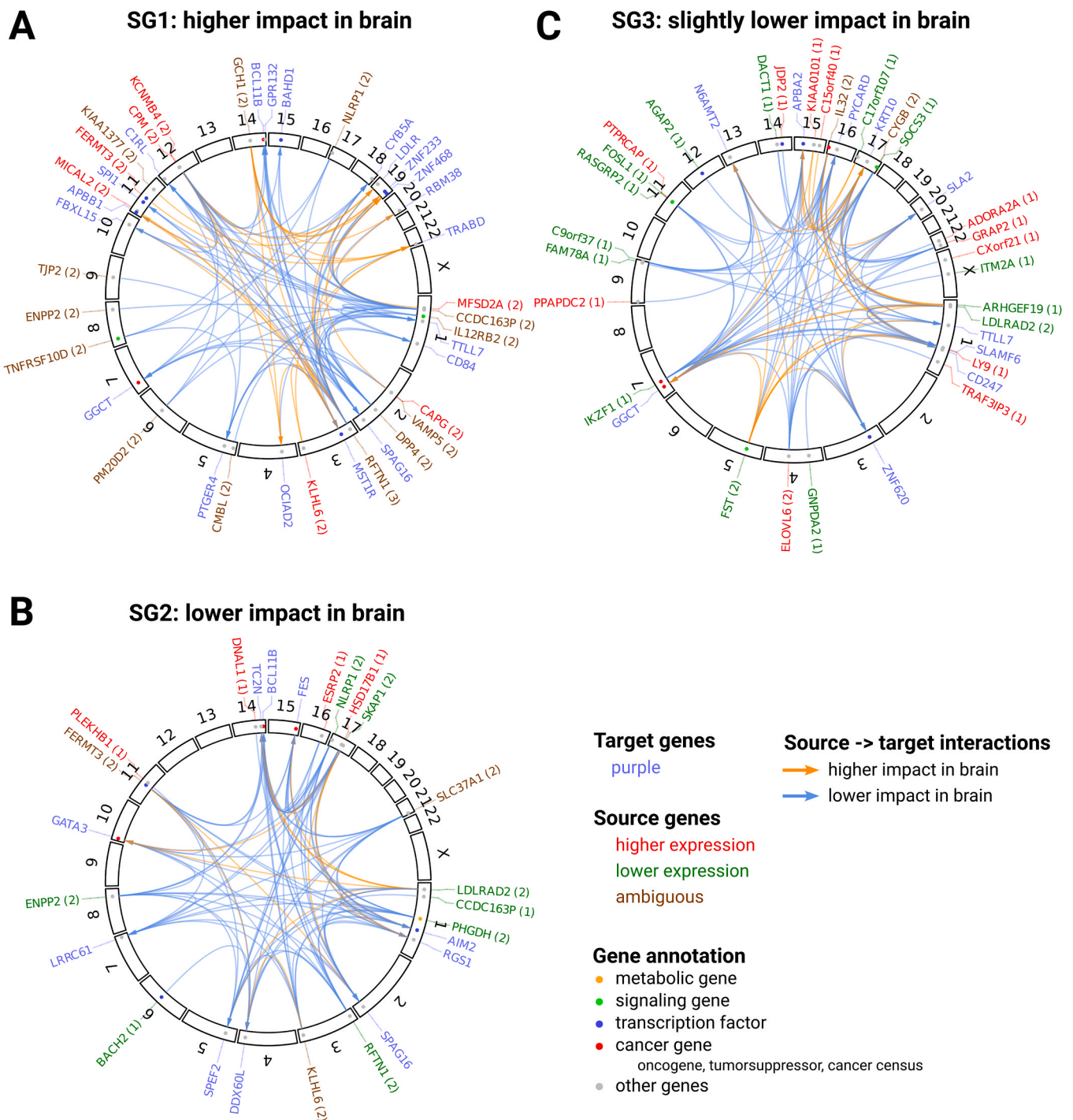


**Fig. 5.** Subgroup-specific accumulation of top impacts from potential driver genes on target genes. The circos plots visualize selected impacts for each of the three revealed subgroups SG1, SG2, and SG3 that flow through the learned melanoma-specific gene regulatory network from potential driver genes to target genes. The included target genes (purple) either received higher (orange interaction arrows) or lower (blue interaction arrows) impacts in the brain metastasis compared to the corresponding extracranial metastasis from the corresponding potential driver genes of specific patient-matched metastasis pairs of each subgroup. The shown top genes were selected by their co-occurrence in the metastasis pair of a specific subgroup and their magnitude of the impact ratio between brain and extracranial metastases in our melanoma metastasis discovery cohort (see Methods for details). The driver genes are either more highly expressed (red) or more lowly expressed (green) in the brain compared to the patient-matched extracranial metastasis of a subgroup, or ambiguous (brown). Numbers in brackets behind the gene names indicate the number of metastasis pairs in which a gene occurred in. General functions of driver and target genes are annotated with colored dots. Detailed data are in Table S10.

*SLAMF6* of SG3 is a potential new target for immunotherapy against melanoma [70]. *PYCARD* is involved in inflammatory and apoptotic signaling [62]. It is down-regulated in metastatic melanoma [71] and its expression is prognostic for effectiveness of anti-PD-1 immunotherapy in melanoma [72].

### 3.7. Validation of impact subgroups and subgroup specific target genes

Gene expression profiles of an additional cohort of nine patient-matched brain and extracranial metastasis pairs were available for an independent validation (Table S15, validation cohort). The TCGA-based

**Table 3**

Most promising candidate target genes of each subgroup. Biological functions were taken from [genecards.org](http://genecards.org). Last column lists the literature references with the highest relevance for melanoma. The full list of all candidate genes is given in [Table S11](#).

Gene	Chromosome	Subgroup	Mean log2 impact ratio	Mean log2 expression ratio	Biological function	Melanoma references
<i>RBM38</i>	chr20	SG1 - higher	0.71	-0.20	DNA damage response, regulation of proliferation	[63]
<i>BCL11B</i>	chr14	SG1 - higher	-0.45	-2.26	transcription regulation, nucleosome and histone	[64,65]
		SG2 - lower	-1.76	-1.28	regulation, T cell identity	
<i>AIM2</i>	chr1	SG2 - lower	-1.92	-0.71	cell proliferation	[66,95]
<i>FES</i>	chr15	SG2 - lower	-1.94	-0.95		[67,68]
<i>GATA3</i>	chr10	SG2 - lower	-1.76	-1.12	transcription factor, regulator of T-cell development	[69,96]
<i>SLAMF6</i>	chr1	SG3 - slightly lower	-0.76	-1.93	immunoglobulin, NK cell activation	[70,97]
<i>PYCARD</i>	chr16	SG3 - slightly lower	-0.77	-0.33	inflammatory and apoptotic signaling, activates caspase	[71,72,98,99]

gene regulatory network showed equally good predictive performance for both the validation and the discovery cohort (Fig. 2A), also when stratifying into brain and extracranial metastases (Fig. 2B). Impact ratio analyses were performed with the same TCGA-based gene regulatory networks as for the discovery cohort with the exception that no promoter methylation data was available (see Methods for details). Genome-wide impact log<sub>2</sub>-ratios were obtained for each patient-matched metastasis pair of the validation cohort. Then, a joint hierarchical clustering was performed with the profiles of the discovery and validation cohort. The nine validation pairs clustered closely together with the pairs of the initial discovery cohort that formed the subgroups SG2 and SG3 (Fig. S9). Thus, the validation metastasis pairs belong either to SG2 or SG3, which clearly supports the existence of these two subgroups. Again, a stability analysis was done with *pvclust* that showed that the subgroups from this joint clustering were fully stable (Fig. S9: AU values 96–100 at the root nodes of subgroups). Further, subgroup-specific consistent target genes were determined for the subgroups SG2 and SG3 of the validation cohort in the same way as for the discovery cohort. The target genes were also ranked by their impact log<sub>2</sub>-ratios. Nine of ten (SG2) and five of ten (SG3) target genes that were identified with the discovery cohort were also part of the validation ranking lists. Moreover, ten of these genes were also ranked at the top of the lists (SG2: *AIM2*, *BCL11B*, *FES*, *GATA3*, *RGS1*, *SPAG16*, *TC2N*, SG3: *GGCT*, *KRT10*, *ZNF620*), as observed in the ranking of the discovery cohort (Table S14, percentiles of genes < 15 %). Thus, the subgroup-specific target genes between the validation and the discovery cohort showed a good overlap. This further supports that the reported target genes may contribute to the establishment of the observed subgroups.

#### 4. Discussion

Melanoma presents an ongoing, huge burden for patients and society [1]. Melanoma brain metastases are particularly difficult to treat [73]. A deeper understanding of molecular mechanisms is needed to develop new prognostic and therapeutic tools. We here contributed to this field by presenting an innovative computational analysis of 11 patient-matched brain and extracranial melanoma metastasis pairs. Melanomas are highly individual tumors because of their elevated mutation rate [4]. Therefore, we decided against a mere description of methylation and expression differences and instead performed an integrative analysis of promoter methylation and gene expression data with the help of a specifically developed network-based approach. Thus, starting with highly individual, heterogeneous driver gene candidates of patient-matched metastasis pairs, the network-based analysis allowed us to discover three homogeneous subgroups and corresponding subgroup-specific downstream targets.

The basis of the presented analysis were genome-wide melanoma-specific gene regulatory networks inferred from the large TCGA melanoma cohort. Thereby, the expression of each gene was modeled as a linear combination of its promoter methylation and the expression levels

of all other genes adapting the basic approach by Seifert et al. [39,40]. The obtained networks were well-suited to predict the expression behavior of genes in independent test data sets, clearly showing that predictive connections between genes were captured. The networks also showed good power for the prediction of the expression behavior of most genes in our small discovery and validation cohorts of patient-matched melanoma metastasis pairs, whose data were measured on different experimental platforms than the TCGA cohort. Although the predictive power was slightly reduced in comparison to the TCGA test data, it still demonstrated that the obtained networks generalized well across cohorts with different patients and technologies. Moreover, even though the training cohort contained only one brain metastasis, the observation of the good predictive power for our melanoma discovery and validation cohort was in accordance with prior findings that networks learned with *regNet* are able to generalize well, even across tumor entities [39]. Thus, the networks learned on public TCGA data represented a valuable basis for our analysis. This is also supported by the fact that known melanoma driver genes were well embedded in the network and ranked among the top connected genes.

Both metastases of each patient-specific pair were compared and driver gene candidates with differential promoter methylation and opposed expression were determined. Unfortunately, the obtained gene sets only barely overlapped between patients. However, this was an ideal motivation and starting point to perform an analysis of individual patient-matched metastasis pairs with the help of the learned networks. We applied the networks to elucidate which downstream target genes and pathways were affected by the potential driver gene candidates. The impacts of each driver candidate on all other genes were determined for each patient-matched metastasis pair. The impact ratios obtained by comparing a brain with its corresponding extracranial metastasis yielded patient-specific impact profiles. Hierarchical cluster analysis of these profiles allowed metastasis pairs to be classified into three robust subgroups. Bootstrap resampling validated the reliability of the subgroups. This was critical given the relatively small cohort size when assessing the universality of subgroups. The revealed subgroups had rather higher (SG1), slightly lower (SG3) and lower average impact ratios (SG2) on known pathways in the brain metastases. A higher impact ratio means that the potential driver genes had a higher influence on the expression of the pathways in the brain compared to the extracranial metastasis of a patient. A lower impact ratio means, the expression of the pathway was more independent of the potential driver genes in the brain metastasis of the patient. The patterns of higher or lower impact ratios were of global nature, that is, almost all pathways were affected in the same way within a metastasis pair. As these were marked global differences, subsequent analyses were performed on a subgroup comparison basis.

The presented pathway analyses uncovered regulatory differences of the subgroups. Subgroups SG2 and SG3 had lower average impacts on pathways in the brain metastases. Cell proliferation was overrepresented in SG2. This hints at a reduced control of cellular growth, a major

characteristic of cancers. Regulation of proteolysis, a process involved in tumor progression and metastases [74,75], was also overrepresented. Cytokine receptor activity was overrepresented in SG3. Melanoma modulate immune cells in the tumor micro-environment by excreting cytokines that affect regulatory T cells and dendritic cells [8]. The SG1 subgroup had many more subgroup-specific overrepresented GO terms, including cytokine and interferon I signaling from target genes with higher impact in the brain metastases. The application of the cytokine interleukin-2 was an early, moderately successful treatment option for metastatic melanoma, and combinations with other cytokines and modern therapies have been explored [76]. More targeted delivery using oncolytic viruses is still being investigated [77]. Terms from genes with lower impact in SG1 brain metastases included migration of diverse immune cells, mast cell activity, myeloid cell differentiation, (neuro) inflammatory response and glial cell activation. The lower impact in brain metastases could provide a potential hint to a reduced control of the adaptive immunity and rather uncontrolled inflammation-like processes. Neuroinflammation and the tumor micro-environment are increasingly thought to play a role in brain tumors and metastases [78]. Distinct glial and myeloid cells were shown to have immunosuppressive and tumor-promoting effects in brain tumors and glioma [79]. Gonzalez et al. proposed the coexistence of an inflammatory and a proliferative archetype in brain metastases, which was derived from single cell analyses [25]. The inflammatory archetype may be more active in the subgroup SG1 discovered here. PI3K signaling was another overrepresented term of the subgroup SG1. PI3K regulates many cellular functions including growth, proliferation, survival and migration and is often dysregulated in cancer [80]. The PI3K/AKT pathway is upregulated in melanoma brain compared to matched extracranial metastases [15,16]. Its inhibition may resensitize brain metastases to BRAF inhibitors [16] and control melanoma brain metastases growth [23]. The PI3K/AKT/mTOR pathway plays a key role in early metastatic colonization of the brain in melanoma, and drug intervention may even help to prevent the formation of brain metastases [81]. Calcium ion transport was also overrepresented in the subgroup SG1. Recent studies have uncovered the role of calcium signaling in brain tumor proliferation, resistance and metastasis [82,83]. Several *in vitro* and xenograft studies have shown that blocking of T-type calcium channels can reduce viability, migration and invasion of melanoma cells, and may be a new strategy against melanoma progression and therapy resistance [84].

To uncover the significance of changed impacts on gene sets, we looked at the relationship of impact and expression ratios between the brain and extracranial metastases. There was a global tendency that pathways with higher impact ratios had lower expression ratios in all subgroups. However, there were different trends in the pathways of the subgroup SG1 on the one hand and the subgroups SG2 and SG3 on the other hand. The latter two often behaved similar throughout this study. For example, citrate and pyruvate metabolism and the pentose phosphate pathway (PPP) showed higher transcription in the brain metastases of all subgroups. Still, the underlying regulation seems to be very complex, because higher impacts on these pathways was observed for SG1 and lower impacts were observed for SG2 and SG3. Upregulation of the PPP enables tumors to switch to aerobic glycolysis [85], and to counteract the elevated oxidative stress [85,86]. In melanoma, PPP is involved in conferring metastatic potential, manages oxidative stress [87], and also contributes to therapy resistance [88]. An *in vitro* therapeutic intervention that downregulated PPP showed potential for a resensitisation to melanoma treatment [88].

Another interesting finding was a lower expression of many immune cell differentiation and signaling pathways in all subgroups comparing brain and extracranial metastases. While these pathways experienced a higher regulatory impact in brain metastases of subgroup SG1, there was a reduced impact on these pathways in subgroups SG2 and SG3. These findings suggest that all brain metastases experience transcriptional hindrance of immune processes, but the underlying regulation differs between the three subgroups. Our findings are supported by Fischer

et al. who also reported immunosuppression comparing patient-matched brain and extracranial melanoma metastases [21]. Melanoma can develop various immune escape strategies including blocking of T-cell activation via PD-1/PD-L1 interaction [8]. This is also well supported in our data by the observation that the PD-1/PD-L1 pathway was more lowly expressed in brain metastases in almost all cases. Corresponding clinical trials with PD-1/PD-L1 checkpoint inhibitors have shown promising results in patients with melanoma brain metastases [89].

This motivated us to obtain a more detailed view on the changed impacts between patient-matched metastasis pairs by determining subgroup-specific target genes with consistently highly differential impacts between brain and extracranial metastases. While the initially determined transcriptional driver candidates were nearly exclusive for individual patients, the target candidate genes represented their regulatory consequences with higher relevance for a patient subgroup. Importantly, the role in cancer was demonstrated in several studies for nearly all target candidates, and half of them showed relevant studies in melanoma (Appendix A, Table S13).

Overall, functions in innate immunity, and lymphocyte development and activation were frequently associated with the predicted target genes of all three subgroups. Melanoma can modulate their micro-environment with immune signals [7], and enriched categories related to chemokines also indicate this for our cohort. This is also supported by other studies that showed that melanoma brain metastases that suppress immune reactions have a worse prognosis and that heterogeneous immune infiltration correlates with survival [21]. Focusing on the three revealed subgroups, predicted target genes of subgroup SG1 were frequently involved in transcriptional regulation and some also showed associations with melanoma [62,90–92]. Promising target genes of subgroup SG2 are known to be involved in melanoma invasion (*FES* [67], *GATA3* [69]) and in immune response in diverse tumors (*BCL11B* [65], *AIM2* [66]). Predicted promising target genes of subgroup SG3 are known to be involved in melanoma immune response (*SLA2* [93], *SLAMF6* [70]) and metastasis formation (*CD247* [94], *PYCARD* [71]). Thus, each of the three revealed subgroups is potentially influenced by genes that could represent promising targets for future experimental studies.

Further, the multiple metastasis pairs of each of the three patients P08, P18 and P42 showed a quite interesting behavior concerning the subgroups-specific pathway clustering. They were part of our study, because an experienced pathologist had marked histologically distinct regions in the extracranial metastases of these patients. Such distinct regions may result from different subclones within a metastasis. They can show different pathway activities, which were confirmed for all three patients. All their pairs were assigned to different subgroups. The two pairs of patient P18 were in SG2 and SG3. The two pairs of patient P42 were in SG1 and SG2. The three pairs of patient P08 were even distributed across all three subgroups SG1, SG2 and SG3. Since especially the pathway impact profiles of SG1 were clearly different from those of SG2 and SG3 (Fig. 3), the patients P08 and P42 had pairs that differed more strongly than those of P18. Thus, a brain metastasis and histologically distinct regions of the corresponding matched extracranial metastasis can show varying degrees of pathway differences, which could be an important information for the treatment of both metastasis types.

Globally, a limitation of our study is the small sample size, because patient-matched melanoma metastases are generally difficult to obtain [20] and study cohorts typically range from about 8–40 patients with matched samples [15,16,21]. However, our cohort consists of nearly untreated metastasis pairs, which allows for highly valuable insights, and the personalized analysis of the patient-matched metastasis pairs enabled predictions for each individual patient. Another limitation is that network training had to be performed on a large independent patient cohort with data from different experimental conditions and sequencing platforms, which may reduce the power of discoveries. Additionally, only less than half of the known protein-coding genes

could be included in the analyses, mainly because of the different platforms involved. Finally, the formalin fixation and paraffin embedding of the tissue samples may have introduced artifacts. Despite all these drawbacks, the existence of two of the three subgroups and their characteristic target genes were confirmed by the analysis of metastasis pairs from an independent validation cohort. An extensive literature search and text mining further confirmed the relevance of the findings. For example, the predicted subgroup-specific target genes *RBM38*, *FES* and *GATA3* are known to play a role in melanoma progression and metastasis and the subgroup-specific target genes *AIM2* and *SLAMF6* have already been reported as therapeutic targets in melanoma (Table 3). This indicates the clinical relevance of our findings, and future experimental studies could explore their potential for new treatment strategies for melanoma metastases.

Further, single-cell transcriptome studies of melanoma metastasis are emerging [25,26]. It will be intriguing to see if subgroups of differentially regulated brain metastases can be found when looking into pure tumor cells. Likewise, the role of the diverse immune cells can be discovered with that technology. However, patient-matched single cell melanoma metastasis pairs are not yet available.

In summary, our innovative network-based analysis of patient-matched melanoma metastasis pairs enabled us to determine potential impacts of individual patient-specific driver candidates on downstream genes. The resulting impact profiles allowed us to group the virtually private metastasis pairs into three robust subgroups that were characterized by more actionable target genes that are potentially triggered by the individual driver candidates. Our study has demonstrated how one can go from heterogeneous patient-specific metastases pairs with individual driver candidates down to a limited number of subgroups and their associated subgroup-specific gene alterations. This contributes to a better molecular stratification of melanoma brain metastases and could provide a basis for experimental validation of specific genes. Further, the developed computational network-based data analysis strategy can also be transferred to other types of cancer.

#### Author statement

All authors have seen and approved the final version of the manuscript being submitted. All of the authors declare that this manuscript is original and has not been published before and is not currently being considered for publication elsewhere.

#### CRediT authorship contribution statement

Conceptualization: MS; Investigation and Formal Analysis: KG, MS; Resources and Data Curation: KG, MS, MM, DW and TK; Writing - Original Draft: KG, MS; Writing - Review & Editing: KG, TK, DW, FM, MS; Revision: KG, MS; Funding Acquisition and Supervision: MS, DW, FM.

#### Declaration of Competing Interest

The authors declare that they have no known competing financial interests or personal relationships that could have appeared to influence the work reported in this paper.

#### Acknowledgments

This work was financially supported by the Federal Ministry of Education and Research BMBF e:Med Junior Research Alliance Grants, Germany (KG, TK, DW and MS: 01ZX1913A/B), by an NCT Proof-of-Concept Trial Research Grant, Germany (MS, FM) and by an NCT Translational Research Grant in Precision Oncology, Germany (MS, FM).

## Appendix A. Supporting information

Supplementary data associated with this article can be found in the online version at doi:10.1016/j.csbj.2024.02.013.

## References

- [1] Siegel RL, Miller KD, Jemal A. Cancer statistics, 2020. *CA Cancer J Clin* 2020;70:7–30.
- [2] Michielin O, van Akkooi ACJ, Ascierto PA, Dummer R, Keilholz U. ESMO guidelines committee. electronic address: clinicalguidelines@esmo.org. Cutaneous melanoma: ESMO clinical practice guidelines for diagnosis, treatment and follow-up. *Ann Oncol* 2019;30:1884–901.
- [3] Rebecca VW, Sondak VK, Smalley KSM. A brief history of melanoma: from mummies to mutations. *Melanoma Res* 2012;22:114–22.
- [4] Alexandrov LB, Nik-Zainal S, Wedge DC, Aparicio SAJR, Behjati S, Biankin AV, et al. Signatures of mutational processes in human cancer. *Nature* 2013;500:415–21.
- [5] Davis LE, Shalin SC, Tackett AJ. Current state of melanoma diagnosis and treatment. *Cancer Biol Ther* 2019;20:1366–79.
- [6] Dummer R, Flaherty K, Robert C, Arance AM, de Groot JW, Garbe C, et al. Five-year overall survival (OS) in COLUMBUS: a randomized phase 3 trial of encorafenib plus binimetinib versus vemurafenib or encorafenib in patients (pts) with BRAF V600-mutant melanoma. *J Clin Oncol* 2021;39. [https://doi.org/10.1200/JCO.2021.39.15\\_suppl.9507](https://doi.org/10.1200/JCO.2021.39.15_suppl.9507).
- [7] Marzagalli M, Ebel ND, Manuel ER. Unraveling the crosstalk between melanoma and immune cells in the tumor microenvironment. *Semin Cancer Biol* 2019;59:236–50. <https://doi.org/10.1016/j.semcancer.2019.08.002>.
- [8] Eddy K, Chen S. Overcoming immune evasion in melanoma. *Int J Mol Sci* 2020;21:8984.
- [9] Wolchok JD, Chiarion-Sileni V, Gonzalez R, Grob J-J, Rutkowski P, Lao CD, et al. Long-term outcomes with nivolumab plus ipilimumab or nivolumab alone versus ipilimumab in patients with advanced melanoma. *J Clin Oncol* 2022;40:127–37. <https://doi.org/10.1200/JCO.21.02229>.
- [10] Wolchok JD, Chiarion-Sileni V, Gonzalez R, Rutkowski P, Grob J-J, Cowey CL, et al. Overall survival with combined nivolumab and ipilimumab in advanced melanoma. *N Engl J Med* 2017;377:1345–56. <https://doi.org/10.1056/NEJMoa1709684>.
- [11] Davies MA, Liu P, McIntyre S, Kim KB, Papadopoulos N, Hwu WJ, et al. Prognostic factors for survival in melanoma patients with brain metastases. *Cancer* 2011;117:1687–96. <https://doi.org/10.1002/CNCR.25634>.
- [12] Tawbi HA, Forsyth PA, Hodi FS, Algazi AP, Hamid O, Lao CD, et al. Long-term outcomes of patients with active melanoma brain metastases treated with combination nivolumab plus ipilimumab (CheckMate 204): final results of an open-label, multicentre, phase 2 study. *Lancet Oncol* 2021;22:1692–704. [https://doi.org/10.1016/S1470-2045\(21\)00545-3](https://doi.org/10.1016/S1470-2045(21)00545-3).
- [13] Davies MA, Saiag P, Robert C, Grob J-J, Flaherty KT, Arance A, et al. Dabrafenib plus trametinib in patients with BRAFV600-mutant melanoma brain metastases (COMBI-MB): a multicentre, multicohort, open-label, phase 2 trial. *Lancet Oncol* 2017;18:863–73. [https://doi.org/10.1016/S1470-2045\(17\)30429-1](https://doi.org/10.1016/S1470-2045(17)30429-1).
- [14] Eroglu Z, Holmen SL, Chen Q, Khushalani NI, Amaravadi R, Thomas R, et al. Melanoma central nervous system metastases: An update to approaches, challenges, and opportunities. *Pigment Cell Melanoma Res* 2019;32:458–69. <https://doi.org/10.1111/PCMR.12771>.
- [15] Chen G, Chakravarti N, Aardalen K, Lazar AJ, Tetzlaff MT, Wubbenhorst B, et al. Molecular profiling of patient-matched brain and extracranial melanoma metastases implicates the PI3K pathway as a therapeutic target. *Clin Cancer Res* 2014;20:5537–46.
- [16] Niessner H, Forscher A, Klumpp B, Honegger JB, Witte M, Bornemann A, et al. Targeting hyperactivation of the AKT survival pathway to overcome therapy resistance of melanoma brain metastases. *Cancer Med* 2013;2:76–85.
- [17] Ciminera AK, Jandial R, Termini J. Metabolic advantages and vulnerabilities in brain metastases. *Clin Exp Metastasis* 2017;34:401–10.
- [18] Gopal YNV, Rizos H, Chen G, Deng W, Frederick DT, Cooper ZA, et al. Inhibition of mTORC1/2 overcomes resistance to MAPK pathway inhibitors mediated by PGC1 $\alpha$  and oxidative phosphorylation in melanoma. *Cancer Res* 2014;74:7037–47.
- [19] Brastianos PK, Carter SL, Santagata S, Cahill DP, Taylor-Weiner A, Jones RT, et al. Genomic characterization of brain metastases reveals branched evolution and potential therapeutic targets. *Cancer Discov* 2015;5:1164–77.
- [20] Váraljai R, Horn S, Sucker A, Piercianek D, Schmitt V, Carpintero A, et al. Integrative genomic analyses of patient-matched intracranial and extracranial metastases reveal a novel brain-specific landscape of genetic variants in driver genes of malignant melanoma. *Cancers (Basel)* 2021;13:1–16. <https://doi.org/10.3390/CANCERS13040731>.
- [21] Fischer GM, Jalali A, Kircher DA, Lee W-C, McQuade JL, Haydu LE, et al. Molecular profiling reveals unique immune and metabolic features of melanoma brain metastases. *Cancer Discov* 2019;9:628–45.
- [22] In GK, Poorman K, Saul M, O'Day S, Farma JM, Olszanski AJ, et al. Molecular profiling of melanoma brain metastases compared to primary cutaneous melanoma and to extracranial metastases. *Oncotarget* 2020;11:3118–28. <https://doi.org/10.18632/oncotarget.27686>.
- [23] Niessner H, Schmitz J, Tabatabai G, Schmid AM, Calaminus C, Sinnberg T, et al. PI3K pathway inhibition achieves potent antitumor activity in melanoma brain

- metastases in vitro and in vivo. *Clin Cancer Res* 2016;22:5818–28. <https://doi.org/10.1158/1078-0432.CCR-16-0064>.
- [24] Westphal D, Glitza Oliva IC, Niessner H. Molecular insights into melanoma brain metastases. *Cancer* 2017;123:2163–75.
- [25] Gonzalez H, Mei W, Robles I, Hagerling C, Allen BM, Hauge Okholm TL, et al. Cellular architecture of human brain metastases. *Cell* 2022;185(729–745):e20.
- [26] Biermann J, Melms JC, Amin AD, Wang Y, Caprio LA, Karz A, et al. Dissecting the treatment-naive ecosystem of human melanoma brain metastasis. *Cell* 2022;185(2591–2608):e30. <https://doi.org/10.1016/J.CELL.2022.06.007>.
- [27] Moore LD, Le T, Fan G. DNA methylation and its basic function. *Neuropsychopharmacology* 2013;38:23–38.
- [28] Chen JF, Yan Q. The roles of epigenetics in cancer progression and metastasis. *Biochem J* 2021;478:3373–93. <https://doi.org/10.1042/BCJ20210084>.
- [29] Ness C, Katta K, Garred Ø, Kumar T, Olstad OK, Petrovski G, et al. Integrated differential DNA methylation and gene expression of formalin-fixed paraffin-embedded uveal melanoma specimens identifies genes associated with early metastasis and poor prognosis. *Exp Eye Res* 2021;203. <https://doi.org/10.1016/J.EXER.2020.108426>.
- [30] Wouters J, Vizoso M, Martinez-Cardus A, Carmona FJ, Govaere O, Laguna T, et al. Comprehensive DNA methylation study identifies novel progression-related and prognostic markers for cutaneous melanoma. *BMC Med* 2017;15:101.
- [31] Marzese DM, Scolyer RA, Roqué M, Vargas-Roig LM, Huynh JL, Wilcott JS, et al. DNA methylation and gene deletion analysis of brain metastases in melanoma patients identifies mutually exclusive molecular alterations. *Neuro Oncol* 2014;16:1499–509.
- [32] Kraft T, Grützmann K, Meinhardt M, Meier F, Westphal D, Seifert M. Patient-specific identification of genome-wide DNA-methylation differences between intracranial and extracranial melanoma metastases. *Sci Rep* 2023;13. <https://doi.org/10.1038/S41598-022-24940-W>.
- [33] Coghlin C, Murray GI. The role of gene regulatory networks in promoting cancer progression and metastasis. *Future Oncol* 2014;10:735–48.
- [34] Clarke R. Introduction: Cancer gene networks. *Methods Mol Biol* 2017;151:3–19.
- [35] Poornima P, Kumar JD, Zhao Q, Blunder M, Efferth T. Network pharmacology of cancer: From understanding of complex interactomes to the design of multi-target specific therapeutics from nature. *Pharmacol Res* 2016;111:290–302.
- [36] Singh AJ, Ramsey SA, Filtz TM, Kioussi C. Differential gene regulatory networks in development and disease. *Cell Mol Life Sci*. 2018;75:1013–25.
- [37] Cha J, Lee I. Single-cell network biology for resolving cellular heterogeneity in human diseases. *Exp Mol Med* 2020;52:1798–808. <https://doi.org/10.1038/s12276-020-00528-0>.
- [38] Fernandez-Valverde SL, Aguilera F, Ramos-Diaz RA. Inference of developmental gene regulatory networks beyond classical model systems: new approaches in the post-genomic Era. *Integr Comp Biol* 2018;58:640–53. <https://doi.org/10.1093/ICB/ICY061>.
- [39] Seifert M, Friedrich B, Beyer A. Importance of rare gene copy number alterations for personalized tumor characterization and survival analysis. *Genome Biol* 2016;17:204.
- [40] Seifert M, Beyer A. regNet: an R package for network-based propagation of gene expression alterations. *Bioinformatics* 2018;34:308–11.
- [41] Seifert M, Peitzsch C, Gorodetska I, Börner C, Klink B, Dubrovskaya A. Network-based analysis of prostate cancer cell lines reveals novel marker gene candidates associated with radioresistance and patient relapse. *PLoS Comput Biol* 2019;15. <https://doi.org/10.1371/JOURNAL.PCBI.1007460>.
- [42] Gladitz J, Klink B, Seifert M. Network-based analysis of oligodendrogliomas predicts novel cancer gene candidates within the region of the 1p/19q co-deletion. *Acta Neuropathol Commun* 2018;6:49.
- [43] Cancer Genome Atlas Network. Genomic classification of cutaneous melanoma. *Cell* 2015;161:1681–96.
- [44] Westphal D, Meinhardt M, Grützmann K, Schöne L, Steining J, Neuhaus LT, et al. Identification of epigenetically regulated genes distinguishing intracranial from extracranial melanoma metastases. *J Invest Dermatol* 2023. <https://doi.org/10.1016/J.JID.2023.01.011>.
- [45] Ritchie ME, Phipson B, Wu D, Hu Y, Law CW, Shi W, et al. limma powers differential expression analyses for RNA-sequencing and microarray studies. *Nucleic Acids Res* 2015;43:e47.
- [46] McCartney DL, Walker RM, Morris SW, McIntosh AM, Porteous DJ, Evans KL. Identification of polymorphic and off-target probe binding sites on the Illumina Infinium MethylationEPIC BeadChip. *Genom Data* 2016;9:22–4.
- [47] Tibshirani R. Regression shrinkage and selection via the lasso. *J R Stat Soc: Ser B (Methodol)* 1996;58:267–88. <https://doi.org/10.1111/J.2517-6161.1996.TB02080.X>.
- [48] Lockhart R, Taylor J, Tibshirani RJ, Tibshirani R. A significance test for the lasso. *Ann Stat* 2014;42:413–68.
- [49] Marbach D, Costello JC, Küffner R, Vega NM, Prill RJ, Camacho DM, et al. Wisdom of crowds for robust gene network inference. *Nat Methods* 2012;9:796–804. <https://doi.org/10.1038/NMETH.2016>.
- [50] Ghanbarian AT, Hurst LD. Neighboring genes show correlated evolution in gene expression. *Mol Biol Evol* 2015;32:1748–66.
- [51] Kamburov A, Pentchev K, Galicka H, Wierling C, Lehrach H, Herwig R. ConsensusPathDB: toward a more complete picture of cell biology. *Nucleic Acids Res* 2011;39:D712–7.
- [52] Mikhaylenko N, Wahnschaffe L, Herling M, Roeder I, Seifert M. Computational gene expression analysis reveals distinct molecular subgroups of T-cell prolymphocytic leukemia. *PLoS One* 2022;17. <https://doi.org/10.1371/JOURNAL.PONE.0274463>.
- [53] Kanehisa M, Goto S. KEGG: kyoto encyclopedia of genes and genomes. *Nucleic Acids Res* 2000;28:27–30.
- [54] Kolde R. CRAN - Package pheatmap 219AD. (<https://cran.r-project.org/web/packages/pheatmap/>) (Accessed 24 January 2024).
- [55] Suzuki R, Shimodaira H. Pvcust: an R package for assessing the uncertainty in hierarchical clustering. *Bioinformatics* 2006;22:1540–2.
- [56] Yu G, Wang L-G, Han Y, He Q-Y. clusterProfiler: an R package for comparing biological themes among gene clusters. *OMICS* 2012;16:284–7.
- [57] Faessler E, Hahn U, Schäuble S. GePI: large-scale text mining, customized retrieval and flexible filtering of gene/protein interactions. *Nucleic Acids Res* 2023;51:W237–42. <https://doi.org/10.1093/nar/gkad445>.
- [58] Piñero J, Ramírez-Anguita JM, Sañchú-Pitarch J, Ronzano F, Centeno E, Sanz F, et al. The DisGenet knowledge platform for disease genomics: 2019 update. *Nucleic Acids Res* 2019. <https://doi.org/10.1093/nar/gkz1021>.
- [59] Gu Z, Gu L, Eils R, Schlesner M, Brors B. circlize Implements and enhances circular visualization in R. *Bioinformatics* 2014;30:2811–2. <https://doi.org/10.1093/BIOINFORMATICS/BTU393>.
- [60] Ku H-C, Cheng C-F. Master regulator activating transcription factor 3 (ATF3) in metabolic homeostasis and cancer. *Front Endocrinol (Lausanne)* 2020;11:556.
- [61] Gupta R, Janostiak R, Wajapeyee N. Transcriptional regulators and alterations that drive melanoma initiation and progression. *Oncogene* 2020;39:7093–105.
- [62] Stelzer G, Rosen N, Plaschkes I, Zimmerman S, Twik M, Fishilevich S, et al. The GeneCards suite: From gene data mining to disease genome sequence analyses. *Curr. Protoc. Bioinforma.* 2016;54:1.30.1–1.30.33.
- [63] Liu J, Xu J, Luo B, Tang J, Hou Z, Zhu Z, et al. Immune landscape and an RBM38-associated immune prognostic model with laboratory verification in malignant melanoma. *Cancers (Basel)* 2022;14. <https://doi.org/10.3390/cancers14061590>.
- [64] Li P, Burke S, Wang J, Chen X, Ortiz M, Lee S-C, et al. Reprogramming of T cells to natural killer-like cells upon Bcl11b deletion. *Science* 1979;201(329):85–9.
- [65] Uddin MN, Zhang Y, Harton JA, MacNamara KC, Avram D. TNF- $\alpha$ -dependent hematopoiesis following Bcl11b deletion in T cells restricts metastatic melanoma. *J Immunol* 2014;192:1946–53.
- [66] Fukuda K, Okamura K, Riding RL, Fan X, Afshari K, Haddadi NS, et al. AIM2 regulates anti-tumor immunity and is a viable therapeutic target for melanoma. *J Exp Med* 2021;218. <https://doi.org/10.1084/JEM.20200962>.
- [67] Olvedy M, Tisserand JC, Luciani F, Boeckx B, Wouters J, Lopez S, et al. Comparative oncogenomics identifies tyrosine kinase FES as a tumor suppressor in melanoma. *J Clin Invest* 2017;127:2310–25.
- [68] Revach OY, Sandler O, Samuels Y, Geiger B. Cross-talk between receptor tyrosine kinases AXL and ERBB3 regulates invadopodia formation in melanoma cells. *Cancer Res* 2019;79:2634–48. <https://doi.org/10.1158/0008-5472.CAN-18-2316>.
- [69] Lin M-C, Lin J-J, Hsu C-L, Juan H-F, Lou P-J, Huang M-C. GATA3 interacts with and stabilizes HIF-1 $\alpha$  to enhance cancer cell invasiveness. *Oncogene* 2017;36:4243–52.
- [70] Hajaj E, Eisenberg G, Klein S, Frankenburg S, Merims S, David I, Ben, et al. SLAMF6 deficiency augments tumor killing and skews toward an effector phenotype revealing it as a novel T cell checkpoint. *Elife* 2020;9. <https://doi.org/10.7554/ELIFE.52539>.
- [71] Liu W, Luo Y, Dunn JH, Norris DA, Dinarello CA, Fujita M. Dual role of apoptosis-associated speck-like protein containing a CARD (ASC) in tumorigenesis of human melanoma. *J Invest Dermatol* 2013;133:518–27.
- [72] Lou X, Li K, Qian B, Li Y, Zhang D, Cui W. Pyroptosis correlates with tumor immunity and prognosis. *Commun Biol* 2022;5:917. <https://doi.org/10.1038/s42003-022-03806-x>.
- [73] Sloot S, Chen YA, Zhao X, Weber JL, Benedict JJ, Mulé JJ, et al. Improved survival of patients with melanoma brain metastases in the era of targeted BRAF and immune checkpoint therapies. *Cancer* 2018;124:297–305.
- [74] Sevenich L, Joyce JA. Pericellular proteolysis in cancer. *Genes Dev* 2014;28:2331–47.
- [75] Vizovisek M, Ristanovic D, Menghini S, Christiansen MG, Schuerle S. The tumor proteolytic landscape: a challenging frontier in cancer diagnosis and therapy. *Int J Mol Sci* 2021;22:1–30. <https://doi.org/10.3390/IJMS22052514>.
- [76] Jiang T, Zhou C, Ren S. Role of IL-2 in cancer immunotherapy. *Oncimmunology* 2016;5:e1163462. <https://doi.org/10.1080/21626402X.2016.1163462>.
- [77] Wang H, Borlongan M, Hemminki A, Basnet S, Sah N, Kaufman HL, et al. Viral vectors expressing interleukin 2 for cancer immunotherapy. *Hum Gene Ther* 2023;34:878–95. <https://doi.org/10.1089/hum.2023.099>.
- [78] Schulz M, Salamero-Boix A, Niesel K, Alekseeva T, Sevenich L. Microenvironmental regulation of tumor progression and therapeutic response in brain metastasis. *Front Immunol* 2019;10:1713. <https://doi.org/10.3389/FIMMU.2019.01713>.
- [79] Andersen BM, Faust Akl C, Wheeler MA, Chiozza EA, Reardon DA, Quintana FJ. Glial and myeloid heterogeneity in the brain tumour microenvironment. *Nat Rev Cancer* 2021;21:786–802. <https://doi.org/10.1038/S41568-021-00397-3>.
- [80] Rodgers SJ, Ferguson DT, Mitchell CA, Ooms LM. Regulation of PI3K effector signalling in cancer by the phosphoinositide phosphatases. *BioSci Rep* 2017;7:37.
- [81] Tehranian C, Fankhauser L, Harter PN, Ratcliffe CDH, Zeiner PS, Messmer JM, et al. The PI3K/Akt/mTOR pathway as a preventive target in melanoma brain metastasis. *Neuro Oncol* 2022;24:213–25. <https://doi.org/10.1093/neuonc/noab159>.
- [82] Maklad A, Sharma A, Azimi I. Calcium signaling in brain cancers: roles and therapeutic targeting. *Cancers (Basel)* 2019;11. <https://doi.org/10.3390/CANCERS11020145>.
- [83] Hausmann D, Hoffmann DC, Venkataramani V, Jung E, Horschitz S, Tetzlaff SK, et al. Autonomous rhythmic activity in glioma networks drives brain tumour growth. *Nature* 2023;613:179–86. <https://doi.org/10.1038/S41586-022-05520-4>.

- [84] Barceló C, Sisó P, Maiques O, de la Rosa I, Martí RM, Macià A. T-type calcium channels: a potential novel target in melanoma. *Cancers (Basel)* 2020;12:391. <https://doi.org/10.3390/cancers12020391>.
- [85] Ghanem N, El-Baba C, Araj K, El-Khoury R, Usta J, Darwiche N. The pentose phosphate pathway in cancer: regulation and therapeutic opportunities. *Chemotherapy* 2021;66:179–91. <https://doi.org/10.1159/000519784>.
- [86] Ge T, Yang J, Zhou S, Wang Y, Li Y, Tong X. The role of the pentose phosphate pathway in diabetes and cancer. *Front Endocrinol (Lausanne)* 2020;11. <https://doi.org/10.3389/FENDO.2020.00365>.
- [87] Tasdogan A, Faubert B, Ramesh V, Ubellacker JM, Shen B, Solmonson A, et al. Metabolic heterogeneity confers differences in melanoma metastatic potential. *Nature* 2020;577:115–20. <https://doi.org/10.1038/s41586-019-1847-2>.
- [88] Wang L, Otkur W, Wang A, Wang W, Lyu Y, Fang L, et al. Norcantharidin overcomes vemurafenib resistance in melanoma by inhibiting pentose phosphate pathway and lipogenesis via downregulating the mTOR pathway. *Front Pharmacol* 2022;13. <https://doi.org/10.3389/FPHAR.2022.906043>.
- [89] Fares J, Ulasov I, Timashev P, Lesniak MS. Emerging principles of brain immunology and immune checkpoint blockade in brain metastases. *Brain* 2021; 144:1046–66. <https://doi.org/10.1093/brain/awab012>.
- [90] Wang J, Li L, Liu S, Zhao Y, Wang L, Du G. FOXC1 promotes melanoma by activating MST1R/PI3K/AKT. *Oncotarget* 2016;7:84375–87.
- [91] Lv L, Wei Q, Wang Z, Zhao Y, Chen N, Yi Q. Clinical and molecular correlates of NLRC5 expression in patients with melanoma. *Front Bioeng Biotechnol* 2021;9. <https://doi.org/10.3389/FBIOE.2021.690186>.
- [92] Wu L, Hu X, Dai H, Chen K, Liu B. Identification of an m6A regulators-mediated prognosis signature for survival prediction and its relevance to immune infiltration in melanoma. *Front Cell Dev Biol* 2021;9. <https://doi.org/10.3389/FCELL.2021.718912>.
- [93] Cerkovnik P, Novaković BJ, Stegel V, Novaković S. Changes in expression of genes involved in antitumor immunity in mice vaccinated with tumor vaccine composed of irradiated syngeneic tumor cells and CpG oligodeoxynucleotides. *Mol Immunol* 2016;79:1–13.
- [94] Rabinowich H, Banks M, Reichert TE, Logan TF, Kirkwood JM, Whiteside TL. Expression and activity of signaling molecules in T lymphocytes obtained from patients with metastatic melanoma before and after interleukin 2 therapy. *Clin Cancer Res* 1996;2:1263–74.
- [95] Zhu H, Zhao M, Chang C, Chan V, Lu Q, Wu H. The complex role of AIM2 in autoimmune diseases and cancers. *Immun Inflamm Dis* 2021;9:649–65. <https://doi.org/10.1002/IID3.443>.
- [96] Riker AI, Enkemann SA, Fodstad O, Liu S, Ren S, Morris C, et al. The gene expression profiles of primary and metastatic melanoma yields a transition point of tumor progression and metastasis. *BMC Med Genom* 2008;1:13. <https://doi.org/10.1186/1755-8794-1-13>.
- [97] Hajaj E, Zisman E, Tzaban S, Merims S, Cohen J, Klein S, et al. Alternative splicing of the inhibitory immune checkpoint receptor SLAMF6 generates a dominant positive form, boosting t-cell effector functions. *Cancer Immunol Res* 2021;9: 637–50. <https://doi.org/10.1158/2326-6066.CIR-20-0800>.
- [98] Okada N, Fujii C, Matsumura T, Kitazawa M, Okuyama R, Taniguchi S, et al. Novel role of ASC as a regulator of metastatic phenotype. *Cancer Med* 2016;5:2487–500. <https://doi.org/10.1002/cam4.800>.
- [99] Strickler AG, Vasquez JG, Yates N, Ho J. Potential diagnostic significance of HSP90, ACS/TMS1, and L-plastin in the identification of melanoma. *Melanoma Res* 2014;24:535–44. <https://doi.org/10.1097/CMR.0000000000000115>.